PAPER • **OPEN ACCESS**

Can mesoscale models capture the effect from cluster wakes offshore?

To cite this article: Miguel Sanchez Gomez *et al* 2024 *J. Phys.: Conf. Ser.* **2767** 062013

Journal of Physics: Conference Series **2767** (2024) 062013 doi:10.1088/1742-6596/2767/6/062013

Can mesoscale models capture the effect from cluster wakes offshore?

Miguel Sanchez Gomez[1], Georgios Deskos[1], Julie K. Lundquist[1,2] and Timothy W. Juliano[3]

[1] National Renewable Energy Laboratory, Golden, Colorado, USA
[2] University of Colorado, Boulder, Colorado, USA
[3] U.S. NSF National Center for Atmospheric Research, Boulder, Colorado, USA

E-mail: [redacted]

Abstract. Long wakes from offshore wind turbine clusters can extend tens of kilometers downstream, affecting the wind resource of a large area. Given the ability of mesoscale numerical weather prediction models to capture important atmospheric phenomena and mechanisms relevant to wake evolution, they are often used to simulate wakes behind large wind turbine clusters and their impact over a wider region. Yet, uncertainty persists regarding the accuracy of representing cluster wakes via mesoscale models and their wind turbine parameterizations. Here, we evaluate the accuracy of the Fitch wind farm parameterization in the Weather Research and Forecasting model in capturing cluster-wake effects using two different options to represent turbulent mixing in the planetary boundary layer. To this end, we compare operational data from an offshore wind farm in the North Sea that is fully or partially waked by an upstream array against high-resolution mesoscale simulations. In general, we find that mesoscale models accurately represent the effect of cluster wakes on front-row turbines of a downstream wind farm. However, the same models may not accurately capture cluster-wake effects on an entire downstream wind farm, due to misrepresenting internal-wake effects.

1. Introduction

Wakes from offshore wind turbine clusters, also referred to as cluster wakes, can propagate long distances, reducing the power production of downstream wind farms [1, 2]. Power losses associated with the effect of cluster wakes have historically been underestimated, leading to uncertainty in energy yield estimates [3].

Analytical and numerical models can be used to estimate losses from cluster wakes and reduce uncertainty in wind farms' energy production assessments. Due to their low computational cost, engineering wake models are commonly used to quantify both wake and power losses. However, these simplified models do not account for some key physical mechanisms that can modify wake evolution in an offshore environment [4, 5]. High-fidelity simulations, like large-eddy simulations (LES), can provide a more complete representation of wake physics [6]; however, at a considerably higher computational cost. Mesoscale numerical weather prediction models, on the other hand, represent well the physical conditions (such as atmospheric stability) that may impact wake evolution—and at a lower computational cost than LES. Nevertheless, uncertainty persists regarding the precision of mesoscale models in accurately representing the impact of wind turbines in the atmospheric boundary layer [7, 8, 9, 10].

Mesoscale simulations rely on the assumption that the size of the most energetic turbulent structures (l) is much smaller than the horizontal grid spacing (Δx) of the model (i.e., $\Delta x >> l$); as such, the effects of turbulence are parameterized. Vertical turbulence mixing at the subgrid scale is typically modeled by assuming horizontal homogeneity using planetary boundary-layer (PBL) parameterizations. In coarse mesoscale simulations ($\Delta x \sim 10$ km), the horizontal gradients of momentum and heat are small compared to their vertical gradients. However, in high-resolution mesoscale simulations ($\Delta x \sim l$), commonly referred to as *gray zone* or *terra incognita* simulations, the most energetic turbulent eddies are not fully parameterized and horizontal gradients of mean quantities become important [11, 12, 13]. Wind turbine and wind farm wakes are characterized by large horizontal and vertical momentum gradients. Consequently, horizontal gradients of turbulence statistics become non-negligible and the three-dimensional effects of turbulence should be considered. In addition, turbine-scale effects (i.e., momentum extraction and enhanced turbulence mixing), which are on the order of 100 m, must also be parameterized. Wind turbines in mesoscale models are typically parameterized as momentum sinks, such as in the Fitch Wind Farm Parameterization (WFP) [14] and the Explicit Wake Parameterization (EWP) [15], or as enhanced surface roughness [16], which misrepresents the wake structure downstream of the turbines [17].

In this study, we evaluate the ability of the Fitch WFP to represent wakes from offshore wind turbines. In particular, we investigate its ability—when used in conjunction with two different PBL schemes, namely the MYNN [18] and the three-dimensional (3D) PBL [13, 19] schemes—to estimate power losses due to external and internal wakes as compared with operational data from an offshore wind farm. The remainder of this paper is organized as follows. In Section 2, we describe the wind farm operational data used to validate the mesoscale simulations. Section 3 provides an overview of the numerical methods employed herein. The climatology of winds around the wind farms of interest is outlined in Section 4. The effects of cluster wakes on downstream wind farms is detailed in Section 5, and a summary and next steps are provided in Section 6.

2. Wind turbine power data

We use wind turbine operational data from offshore wind farms in the North Sea to validate cluster-wake effects in mesoscale models. Specifically, we assess the interaction between the Westermost Rough and Humber Gateway wind farms. Westermost Rough is located approximately 19 km northwest of the Humber Gateway wind farm (Figure 1). The Westermost Rough wind farm comprises 35 Siemens 6-MW wind turbines with hub height at 102 m and 154-m rotor diameter. The Humber Gateway wind farm comprises 73 Vestas 3-MW wind turbines with hub height at 80 m and 112-m rotor diameter. Turbine power data from the Supervisory Control and Data Acquisition system (SCADA) from Westermost Rough between January and December, 2017, are used to validate power production estimates calculated by the mesoscale model. Power production, nacelle wind speed, turbine yaw angle, and fault conditions are provided by the wind farm operator for each turbine as 10-min averages. All turbines in Humber Gateway are assumed to be operating normally for the analysis.

SCADA data filtering is performed using the FLOw Redirection and Induction in Steady State (FLORIS)-based Analysis for SCADA data (FLASC) tool [20]. We filter out power outliers for each turbine based on curtailment, mean-power-curve outliers, sensor-stuck faults, and non-normal operations. On average for all turbines in the wind farm, 77.9% of the data remain valid after discarding outliers. Furthermore, the yaw angle for each turbine is calibrated to true north in FLASC using FLORIS with the Gaussian wake model.

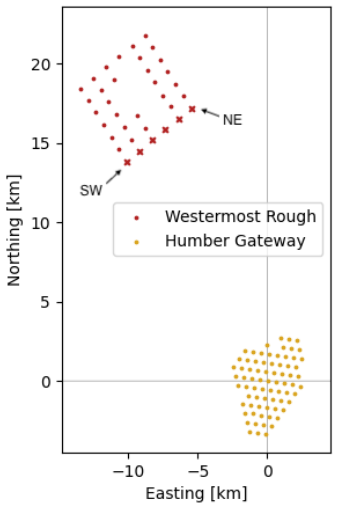

Figure 1. Relative location of the Westermost Rough and Humber Gateway wind farms. Front-row turbines in Westermost Rough for southeasterly winds are shown with crosses. The Southwest (SW) and Northeast (NE) front-row turbines (for southeasterly winds) of Westermost Rough are shown for reference. Relative distances are calculated from the center of the Humber Gateway wind farm.

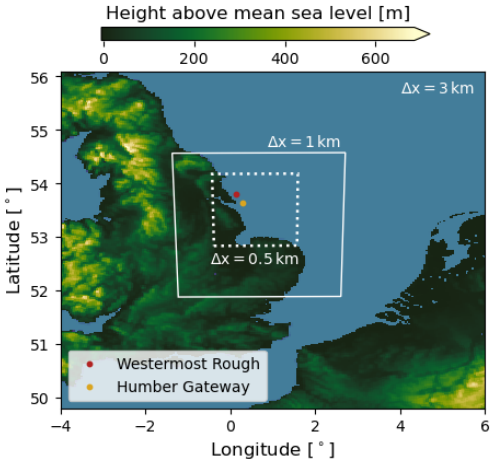

Figure 2. Domain layout for the WRF simulations. The solid and dotted white rectangles represent the location and size of the nested domain for the $\Delta x = 1$ km and $\Delta x = 0.5$ km simulations, respectively, within the parent domain ($\Delta x = 3$ km).

3. Numerical Models

We simulate atmospheric flow around these two wind farms in the North Sea using the Weather Research and Forecasting (WRF) model (Version 4.4) using a two-domain, one-way nesting setup (Figure 2). ERA5 reanalysis [21] provides initial and boundary conditions to the outer ($\Delta x = 3$ km) mesoscale domain. For the nested mesoscale domain, we perform simulations using two horizontal grid spacings, one with $\Delta x = 1$ km (solid white line in Figure 2) and another with $\Delta x = 0.5$ km (dotted white line in Figure 2). The physical characteristics and modeling options of the domains are provided in Table 1.

Two boundary-layer parameterizations are used to model turbulent mixing in the lowest portion of the atmosphere. The one-dimensional 2.5-MYNN boundary-layer parameterization (MYNN from hereafter) [18] is used with $\Delta x = 1$ km, whereas a 3D boundary-layer parameterization (3D PBL from hereafter) [13, 19] is employed with $\Delta x = 0.5$ km. For completeness, we also perform simulations using the 3D PBL for a nested domain with $\Delta x = 1$ km. The MYNN parameterization estimates vertical turbulent mixing using the vertical turbulent stress divergence, whereas horizontal mixing is computed with a Smagorinsky-like approach. In contrast, the 3D PBL explicitly computes both the vertical and horizontal turbulent flux divergence for momentum, heat, and moisture. Here, we use the "boundary-layer approximation" to the 3D PBL, where vertical turbulent fluxes are calculated like in MYNN,

Domain	Δx [km]	Δz_s [m]	(n_x, n_y, n_z)	α [-]	PBL Model
d01	3.0	8	$(241, 241, 79)$	-	MYNN
d02	1.0	8	$(265, 301, 79)$	$[0.0, 0.5, 1.0]$	MYNN
				1.0	3D PBL
	0.5	8	$(265, 301, 79)$	1.0	3D PBL

Table 1. Simulation setup, including horizontal grid resolution (Δx), vertical resolution at the surface (Δz_s), number of grid cells along each direction (n_i), correction factor for the fraction of turbine-added TKE (α), and boundary-layer parameterization for each domain.

and the horizontal turbulent fluxes are calculated analytically following [22], as in [23, 24]. We found the full matrix solution to the turbulent fluxes to be numerically unstable in our test cases. Model closure constants and the master length scale follow the original Mellor–Yamada model [22]. Additional information on the "full" 3D PBL and its "boundary-layer approximation" can be found in Juliano et al. [13].

We simulate the wind turbines exclusively in the nested domain (d02) using the Fitch WFP [14, 25, 23]. The Fitch parameterization represents the effect of wind turbines through a momentum sink and a source of turbulence kinetic energy (TKE). The drag from the turbines on the flow is a function of the thrust coefficient, the number of turbines per grid cell, and the turbine size (i.e., rotor diameter D). The Fitch wind farm parameterization postulates that a fraction of the energy from the flow is converted into increased turbulent motions; thus, the parameterization adds a source to the TKE tendency equation as well. Turbine-added TKE is regulated in the model as $C_{TKE} = \alpha(C_T - C_P)$, where α is a correction factor, and C_T and C_P are the turbine's thrust and power coefficients, respectively, which in turn are a function of inflow wind speed. We explore the sensitivity to the turbine-added TKE in the MYNN simulations by varying α between 0 and 1. Because the average turbine spacing in Westermost Rough and Humber Gateway is 945 m and 580 m, respectively, multiple wind turbines are expected to occupy one grid cell for the $\Delta x = 1$ km domain (Figure 3a). Furthermore, due to the domain discretization and because the effect of the turbines is placed at the grid cell center, the effective wind farm layout of Westermost Rough and Humber Gateway in our simulations (Figure 3) may differ from their physical location (Figure 1). A more accurate representation of each farm's layout is obtained with finer resolution (Figure 3b).

4. Climatology of winds in the region

We characterize the climatology of winds in the region using nacelle-anemometer wind speed and turbine yaw angle (corrected to true north) recorded in SCADA for the turbines in Westermost Rough. Cluster wakes from Humber Gateway are expected to impact Westermost Rough for wind directions between 130° and 170° [26], when both wind farms are partially or fully aligned. Consequently, we focus on these wind sectors. Furthermore, we focus our analysis on winds above cut-in speed and below rated speed (4 m s^{-1} and 13 m s^{-1}, respectively, for the Siemens 6-MW turbine). Rather than replicating the observations on a case-by-case basis, which is highly sensitive to accurately reproducing the temporal evolution of atmospheric conditions, we use ERA5 reanalysis to find times when the statistics of wind speed and direction are comparable to SCADA and simulate those cases in WRF.

To evaluate the capability of mesoscale models in representing cluster wakes, we perform numerical simulations of 42 cases in 2017 that reproduce the statistics of wind speed and direction near the Westermost Rough wind farm. For each case, the parent domain spins up for 14 hr before initializing the nested domain. We discard the first 5 hr of simulation data for the

nested domain. Three-dimensional wind speed and temperature fields, as well as turbine power production, are output every 5 min for 10 hr after spinup of both domains is complete. Note that winds in the mesoscale simulations are expected to be different from the ERA5 reanalysis. ERA5 data is obtained from the ECMWF's Integrated Forecasting System, which employs a different dynamical core, grid resolution, and parameterizations of physical processes from WRF. Thus, even though WRF is forced using ERA5 data, it will reach its own resolved state away from the domain boundaries.

We use the Perkins Skill Score (PSS) [27] to determine a continuous range of wind speeds and directions where wind statistics in the observations and simulations are similar. The PSS is defined as the cumulative minimum value of two distributions of a binned value, measuring the common area between two probability distributions. Here, we compare the conditional probability distributions for wind speed (U_i) and wind direction (ϕ_j) bins from observations (Z_o) and model results (Z_m), as shown in Eq. 1. For the mesoscale simulations, we use wind speed and direction for the grid points closest to the front-row turbines in Westermost Rough.

$$PSS = \sum_{U_i} \sum_{\phi_j} \min\{Z_m(U_i, \phi_j), Z_o(U_i, \phi_j)\} \tag{1}$$

The climatology of winds (i.e., wind speed and direction) near the Westermost Rough wind farm is well represented in the WRF simulations for a range of wind speeds and directions. We calculate the PSS score for different combinations of wind speed and wind direction bins, then find the continuous range of wind speed and directions that maximize the correspondence between the simulations and observations (i.e., PSS score). Note that variations in the cluster-wake effect may influence the model's ability to reproduce the climatology of this site. The PSS score for the conditional probabilities from WRF and SCADA is 0.75 for wind speeds between [6 m s^{-1}, 9.5 m s^{-1}] and wind directions between [130°, 170°], suggesting simulations capture about 75% of the observed probability density functions. Kolmogorov-Smirnov and Chi-Squared tests indicate the statistics of winds in the MYNN and 3D PBL simulations match the statistics of the SCADA data at a 95% confidence level. Moreover, even though the $\Delta x = 0.5$ km domain is smaller than the $\Delta x = 1$ km domain, resulting in different boundary conditions, the statistics of wind speed and direction are still well captured. Approximately 1900 data points of filtered data from SCADA (10-min averages) lay within these wind speed and direction ranges. Similarly, more than 1300 data points from the WRF simulations (data every 5 min) satisfy

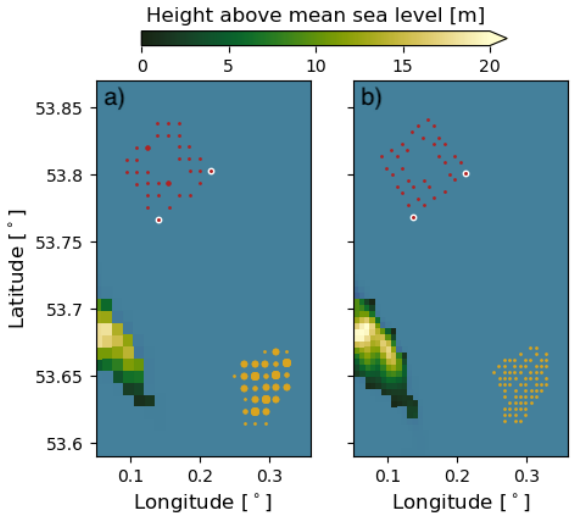

Figure 3. Simulated turbine locations in the WRF grid for the $\Delta x = 1$ km (a) and $\Delta x = 0.5$ km (b) simulations. Multiple turbines located on the same grid cell are represented by larger circles. The edge-most turbines in the front row of Westermost Rough (for southeasterly winds) are highlighted using white circles.

these wind conditions. Note that we use ERA5 reanalysis to find cases when winds at 100 m are between 4 m s^{-1} and 13 m s^{-1}. However, the mesoscale simulations only capture the statistics accurately for wind speeds between 6 m s^{-1} and 9.5 m s^{-1}. The remaining analysis is restricted to winds with a speed between 6 m s^{-1} and 9.5 m s^{-1} and direction between 130° and 170° only.

5. Cluster-wake effects

5.1. Front-row turbines

We quantify cluster-wake effects from Humber Gateway on downstream wind turbines using the average of the ratio of power production from the edge-most, front-row turbines in the Westermost Rough wind farm (turbines SW and NE in Figure 1). This power-ratio metric is accurate for quantifying partially waked conditions for Westermost Rough [26]. The southwest turbine in the front row of Westermost Rough (P_{SW}) is expected to generate more power than the northeast turbine in the front row (P_{NE}) for wind directions around 145°, and vice versa for wind directions around 165° [26].

Mesoscale simulations accurately represent cluster-wake effects on front-row turbines in the Westermost Rough wind farm (Figure 4). In general, all mesoscale simulations display the same trend in the power ratio when compared to SCADA data. The southwest turbine (SW) in Westermost Rough is waked by Humber Gateway for wind direction sectors between 130° and 155°, whereas the northeast turbine (NE) is waked by Humber Gateway for wind direction sectors between 155° and 170°.

The MYNN ($\alpha = 1$) and 3D PBL ($\Delta x = 1$ km) model configurations show the best agreement with the observational data (Figure 4). The power ratio obtained from SCADA is statistically different (95% confidence) from the power ratio predicted using MYNN ($\alpha = 1$) only when the winds have a strong easterly component ($\phi \in [130°, 134°]$). Similarly, SCADA data are only statistically different from the 3D PBL simulations ($\Delta x = 1$ km) for wind sectors $\phi \in [130°, 134°]$ and $\phi = 161° \pm 1°$. Surprisingly, an increased grid resolution while using the 3D PBL (i.e., $\Delta x = 0.5$ km) negatively impacts the ability of the mesoscale model to represent cluster-wake effects on front-row turbines, displaying the least skill in reproducing observations. It is likely that the horizontal gradients of the mean velocities become increasingly important for the wake evolution with the finer grid spacing. Thus, the "full" 3D PBL model instead of its "boundary-layer approximation" may be better suited for modeling the wake evolution downstream of a wind farm using the smaller grid spacing. Despite some studies suggesting turbine-added TKE may affect wind farm wake evolution [25, 23, 8], our data show that power losses due to cluster-wake effects are minimally impacted by α, similar to previous results [28]. Nonetheless, neglecting the turbine-added TKE (i.e., $\alpha = 0$) yields the largest differences between the mesoscale model predictions with MYNN and the SCADA data.

Mesoscale simulations can represent differences in cluster-wake effects caused by different atmospheric stability regimes (Figure 5). For the SCADA data, we quantify stability using the bulk Richardson number between the surface and 150 m derived from ERA5 reanalysis. For WRF, stable conditions are defined using the surface heat flux. For the wind conditions described in Section 4, about 60% (67%) of the cases in WRF (SCADA) are stable and 40% (32%) are unstable. All simulations display increased power losses during stable conditions compared to unstable conditions, just like the SCADA data. The 3D PBL ($\Delta x = 1$ km) better captures cluster-wake effects on front-row turbines for stable and unstable conditions than the other model configurations. Conversely, the 3D PBL ($\Delta x = 0.5$ km) evidences the least agreement with SCADA data for both stable and unstable conditions. Mean cluster-wake effects are similar between the stable and unstable simulations for winds with a strong southerly component ($\phi \sim 165°$). Winds from the south have a long fetch over land, where atmospheric stability can be different (and in many cases opposite) from offshore, and so an internal boundary layer develops with stably stratified winds aloft a weakly unstable surface layer that can persist

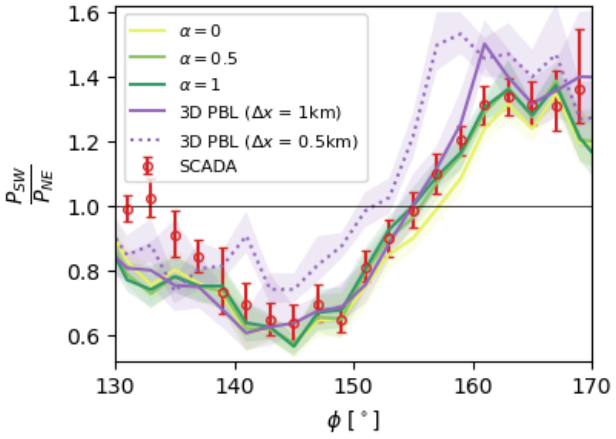

Figure 4. Ratio of power production between the southwest (SW) and northeast (NE) front-row turbines (as shown in Figure 1) of Westermost Rough for simulations and observations. Data are shown for wind speeds between $[6\ \text{m s}^{-1}, 9.5\ \text{m s}^{-1}]$ and wind directions between $[130°, 170°]$ in 2° bins. The shaded area/error bars represent the 95% confidence interval obtained from a bootstrapping method.

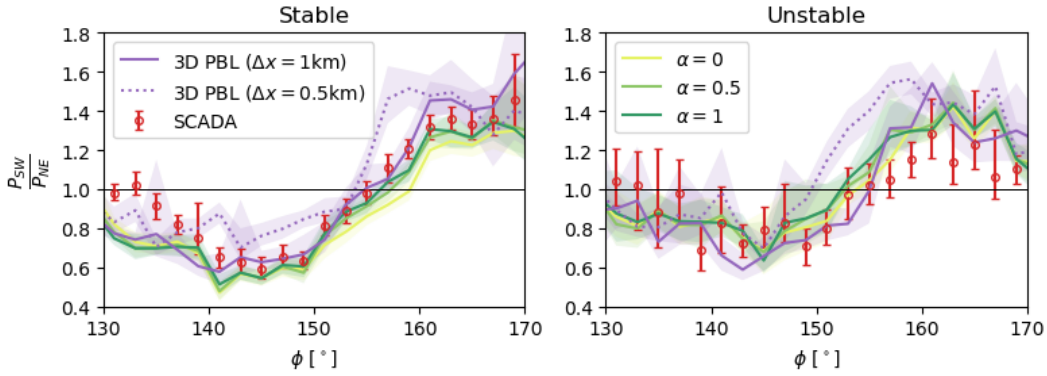

Figure 5. Same as Figure 4 but for stable (left) and unstable (right) atmospheric stability conditions.

for long distances and affect cluster-wake evolution.

5.2. Wind farm

Even though mesoscale simulations accurately represent cluster-wake effects on front-row turbines (Section 5.1), they do not necessarily capture the effect on the entire downstream wind farm. We quantify the model's accuracy in representing the effect from internal and external wakes using the error metric $\mathbb{E}$ defined in Eq. 2, where $\hat{P}_o$ and $\hat{P}_m$ are the average normalized power production of each turbine from SCADA and WRF, respectively, for the wind speed U_i and direction ϕ_j sectors. The normalized power production of each turbine in Westermost Rough for a combination of wind speed and direction (U_i, ϕ_j) is estimated as $\hat{P} = P/P_{FR}$, where P_{FR} is the average power production of the front-row turbines. $\mathbb{E}$ provides a measure of the mismatch between WRF and SCADA for a set of inflow wind conditions. Based on Eq. 2, WRF overestimates wake effects when $\mathbb{E} > 0$, and underestimates wake effects when $\mathbb{E} < 0$. Figure 6 illustrates the mismatch between WRF and SCADA for two sets of wind directions: when the wind turbine columns are aligned with the incoming flow (Figure 6a-c), and when they are staggered (Figure 6d-f). Note that we do not include results from MYNN for $\alpha = 0, 0.5$ in Figure 6 because they are nearly identical to the results from MYNN with $\alpha = 1$.

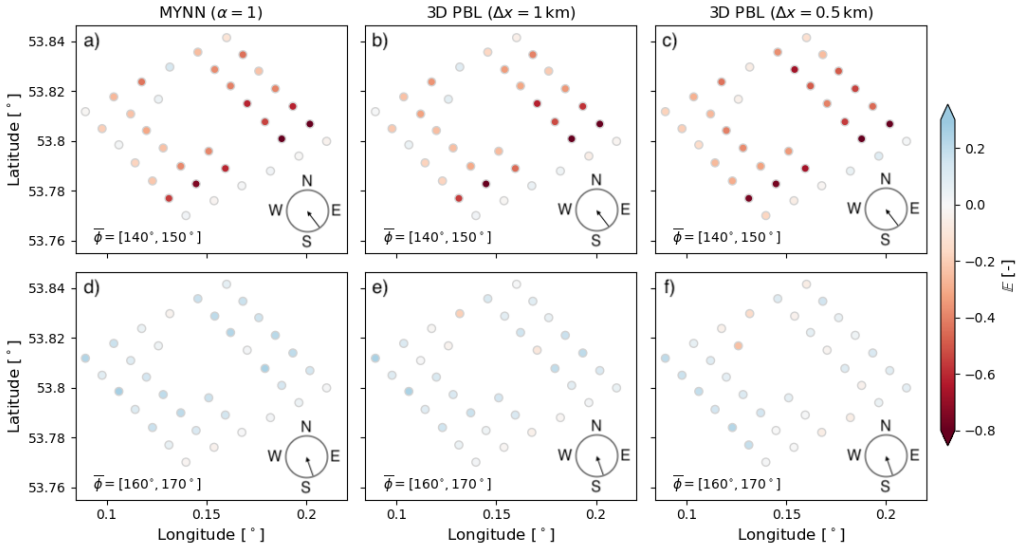

Figure 6. Normalized difference between measured and simulated power production for each wind turbine in Westermost Rough. Data are shown for wind speeds between [6 m s^{-1}, 9.5 m s^{-1}]. The top panels (a-c) correspond to wind directions within [140°, 150°], and the bottom panels (d-f) to wind directions within [160°, 170°]. Panels (a,d) show the difference between SCADA and WRF with MYNN ($\alpha = 1$), panels (b,e) the difference between SCADA and WRF with the 3D PBL ($\Delta x = 1$ km), and panels (c,f) the difference between SCADA and WRF with the 3D PBL ($\Delta x = 0.5$ km). The arrows in the bottom right of each panel illustrate the range of wind directions considered.

$$\mathbb{E}(U_i, \phi_j) = \frac{\hat{P}_o(U_i, \phi_j) - \hat{P}_m(U_i, \phi_j)}{\hat{P}_o(U_i, \phi_j)} \tag{2}$$

Mesoscale simulations underestimate (overestimate) internal-wake effects when the wind direction results in an aligned (staggered) array layout within Westermost Rough (Figure 6). All model configurations display the same trend when compared to the observations. Power production from WRF is generally larger than SCADA for aligned conditions (Figure 6a-c), and consistently larger for the second turbine row in Westermost Rough, suggesting WRF predicts smaller velocity deficits than the observations. Conversely, the simulations predict larger internal-wake velocity deficits when the wind direction results in a staggered layout, as depicted by reduced power production compared to SCADA (Figure 6d-f). Differences between SCADA and WRF are minimal for front-row turbines, as shown in Section 5.1, suggesting cluster wakes from Humber Gateway are accurately represented in the simulations.

Internal-wake effects are not accurately captured in the mesoscale simulations because the velocity deficits are distributed over a grid cell that is much larger than the individual wakes. As a result, the velocity deficit is reduced for aligned conditions ($\phi \approx 146°$), minimizing internal-wake effects on downstream turbines. For the same reasons, power reductions from internal wakes are overestimated in a staggered layout ($\phi \approx 165°$) because individual turbine wakes affect a wider downstream area. Furthermore, turbines may occupy adjacent grid cells in the staggered layout; thus, individual-turbine wakes can propagate to a nearby turbine even if it is not immediately downstream. Given that internal-wake effects are not accurately captured in mesoscale simulations, it can be argued that total wake-related power losses that includes both internal- and cluster-wake effects can be misrepresented.

6. Summary and Conclusions

Wakes from offshore wind turbine clusters can propagate long distances, reducing the power production of downstream wind farms. Power losses from cluster wakes have historically been underestimated, leading to uncertainty in energy yield estimates. Mesoscale numerical weather prediction models can be used to estimate losses from cluster wakes and reduce uncertainty in wind farms' energy production assessments. However, there is still uncertainty regarding the accuracy and calibration parameters of the wind turbine parameterizations within them. Here, we investigate the ability of the mesoscale Fitch wind turbine parameterization to represent offshore cluster wakes using two boundary-layer parameterizations. We perform high-resolution mesoscale simulations of two offshore wind farms in the North Sea using the Weather Research and Forecasting model. Wind turbine operational data from the downstream wind farm are used to investigate the ability of the mesoscale model to capture internal- and external-wake effects.

Mesoscale models accurately represent cluster-wake effects on the front-row turbines of the downstream wind farm, but fail to capture the internal-wake effects. The one-dimensional and three-dimensional boundary-layer parameterizations yield accurate estimates for cluster-wake-induced power losses on the front-row turbines of a waked offshore wind farm (Figure 4). Inherently, stable atmospheric conditions exhibit increased power losses compared to unstable atmospheric stability regimes (Figure 5), a feature that is well-captured by the mesoscale simulations. However, mesoscale models fail to capture the cumulative power reductions for an entire wind farm when it is being waked by an upstream turbine cluster because internal wakes are not well represented. Due to the numerical grid resolution used in the mesoscale simulations, power losses due to internal wakes are overestimated (underestimated) when the wind is staggered (aligned) with the turbine columns of the wind farm (Figure 6). It is likely that an even finer grid spacing is required to accurately represent internal-wake effects in mesoscale simulations. However, the horizontal gradients in the wake of the wind farm may become non-negligible with the smaller grid spacing, highlighting the importance of further development of the "full" 3D PBL for high-resolution mesoscale modeling of wind farms. Future studies could use a hybrid approach and combine engineering models or large-eddy simulations with mesoscale models to evaluate internal-wake effects on power production of the offshore wind farm. Mesoscale models may also be used to estimate cluster-wake effects when observations are not available or for planning purposes. To this end, mesoscale model results may be employed to tune engineering wake models for farm-to-farm wakes for a variety of wind speeds, wind directions, and atmospheric stability conditions that represent the climatology of a given site, which is cost-prohibitive if only using large-eddy simulations.

7. Acknowledgments

The authors would like to thank Ørsted for providing access to operational and measurement data from the Westernmost Rough offshore wind farm. This work was authored in part by the National Renewable Energy Laboratory, operated by Alliance for Sustainable Energy, LLC, for the U.S. Department of Energy (DOE) under Contract No. DE-AC36-08GO28308. Partial funding was provided by DOE's Office of Energy Efficiency and Renewable Energy Wind Energy Technologies Office and funded in part by the Bureau of Ocean Energy Management through an interagency agreement with DOE. Partial funding was also provided by partially funded by the National Offshore Wind Research and Development Consortium (NOWRDC) to carry out a Joint Industry Project investigating Multi-fidelity Modeling of Offshore Wind Inter-array Wake Impacts to Inform Future U.S. Atlantic Offshore Wind Energy Area Development under CRD-23-24539-0. The US government retains certain rights in intellectual property under CRD-23-24539-0. This publication does not necessarily reflect the views of NOWRDC or the US government, and NOWRDC nor the US government makes no representations or

warranties and has no liability for any of its contents. Timothy W. Juliano was supported by the U.S. Department of Energy Wind Technology Office Contract #DE-A05-76RL01830 to Pacific Northwest National Laboratory (PNNL). The National Center for Atmospheric Research (NCAR) is a subcontractor to PNNL under Contract #659135. NCAR is a major facility sponsored by the National Science Foundation under Cooperative Agreement No. 1852977. The research was performed using computational resources sponsored by DOE and located at the National Renewable Energy Laboratory.

References

[1] Platis A, Siedersleben S K, Bange J, Lampert A, Bärfuss K, Hankers R, Cañadillas B, Foreman R, Schulz-Stellenfleth J, Djath B, Neumann T and Emeis S 2018 *Sci Rep* **8** 2163 ISSN 2045-2322
[2] Schneemann J, Rott A, Dörenkämper M, Steinfeld G and Kühn M 2020 *Wind Energ. Sci.* **5** 29–49 ISSN 2366-7451
[3] Lee J C Y and Fields M J 2021 *Wind Energ. Sci.* **6** 311–365 ISSN 2366-7451
[4] Stieren A and Stevens R J 2022 *Flow* **2** E21 ISSN 2633-4259
[5] Doekemeijer B M, Simley E and Fleming P 2022 *Energies* **15** 1964 ISSN 1996-1073
[6] Maas O 2023 *Wind Energ. Sci.* **8** 535–556 ISSN 2366-7451
[7] Eriksson O, Baltscheffsky M, Breton S P, Söderberg S and Ivanell S 2017 *J. Phys.: Conf. Ser.* **854** 012012 ISSN 1742-6588, 1742-6596
[8] Ali K, Schultz D M, Revell A, Stallard T and Ouro P 2023 *Monthly Weather Review* **151** 2333–2359 ISSN 0027-0644, 1520-0493
[9] Fischereit J, Schaldemose Hansen K, Larsén X G, Van Der Laan M P, Réthoré P E and Murcia Leon J P 2022 *Wind Energ. Sci.* **7** 1069–1091 ISSN 2366-7451
[10] Peña A, Mirocha J D and Van Der Laan M P 2022 *Monthly Weather Review* **150** 3051–3064 ISSN 0027-0644, 1520-0493
[11] Wyngaard J C 2004 *Journal of the Atmospheric Sciences* **61** 1816–1826 ISSN 0022-4928, 1520-0469
[12] Rai R K, Berg L K, Kosović B, Haupt S E, Mirocha J D, Ennis B L and Draxl C 2019 *Monthly Weather Review* **147** 1007–1027 ISSN 0027-0644, 1520-0493
[13] Juliano T W, Kosović B, Jiménez P A, Eghdami M, Haupt S E and Martilli A 2022 *Monthly Weather Review* **150** 1585–1619 ISSN 0027-0644, 1520-0493
[14] Fitch A C, Olson J B, Lundquist J K, Dudhia J, Gupta A K, Michalakes J and Barstad I 2012 *Monthly Weather Review* **140** 3017–3038 ISSN 0027-0644, 1520-0493
[15] Volker P J H, Badger J, Hahmann A N and Ott S 2015 *Geosci. Model Dev.* **8** 3715–3731 ISSN 1991-9603
[16] Keith D W, DeCarolis J F, Denkenberger D C, Lenschow D H, Malyshev S L, Pacala S and Rasch P J 2004 *Proc. Natl. Acad. Sci. U.S.A.* **101** 16115–16120 ISSN 0027-8424, 1091-6490
[17] Fitch A C, Olson J B and Lundquist J K 2013 *Journal of Climate* **26** 6439–6458 ISSN 0894-8755, 1520-0442
[18] Nakanishi M and Niino H 2009 *Journal of the Meteorological Society of Japan* **87** 895–912 ISSN 0026-1165, 2186-9057
[19] Kosović B, Jimenez Munoz P, Juliano T W, Martilli A, Eghdami M, Barros A P and Haupt S E 2020 *J. Phys.: Conf. Ser.* **1452** 012080 ISSN 1742-6588, 1742-6596
[20] NREL 2022 Flasc. version 1.0 URL [redacted]
[21] Hersbach H, Bell B, Berrisford P, Biavati G, Horányi A, Muñoz Sabater J, Nicolas J, Peubey C, Radu R, Rozum I, Schepers D, Simmons A, Soci C, Dee D and Thépaut J N 2023 ERA5 hourly data on pressure levels from 1940 to present
[22] Mellor G L and Yamada T 1982 *Reviews of Geophysics* **20** 851–875 ISSN 8755-1209, 1944-9208
[23] Rybchuk A, Juliano T W, Lundquist J K, Rosencrans D, Bodini N and Optis M 2022 *Wind Energ. Sci.* **7** 2085–2098 ISSN 2366-7451
[24] Arthur R S, Juliano T W, Adler B, Krishnamurthy R, Lundquist J K, Kosović B and Jiménez P A 2022 *Journal of Applied Meteorology and Climatology* **61** 685–707 ISSN 1558-8424, 1558-8432
[25] Archer C L, Wu S, Ma Y and Jiménez P A 2020 *Monthly Weather Review* **148** 4823–4835 ISSN 0027-0644, 1520-0493
[26] Nygaard N G, Steen S T, Poulsen L and Pedersen J G 2020 *J. Phys.: Conf. Ser.* **1618** 062072 ISSN 1742-6588, 1742-6596
[27] Perkins S E, Pitman A J, Holbrook N J and McAneney J 2007 *Journal of Climate* **20** 4356–4376 ISSN 1520-0442, 0894-8755
[28] Rosencrans D, Lundquist J K, Optis M, Rybchuk A, Bodini N and Rossol M 2024 *Wind Energ. Sci.* **9** 555–583 ISSN 2366-7443